www.sciencetranslationalmedicine.org/cgi/content/full/6/240/240ra76/DC1

Supplementary Materials for

Chitinase 3–like 1 Suppresses Injury and Promotes Fibroproliferative Responses in Mammalian Lung Fibrosis

Yang Zhou, Hong Peng, Huanxing Sun, Xueyan Peng, Chuyan Tang, Ye Gan, Xiaosong Chen, Aditi Mathur, Buqu Hu, Martin D. Slade, Ruth R. Montgomery, Albert C. Shaw, Robert J. Homer, Eric S. White, Chang-Min Lee, Meagan W. Moore, Mridu Gulati, Chun Geun Lee, Jack A. Elias,* Erica L. Herzog*

*Corresponding author. E-mail: erica.herzog@yale.edu (E.L.H.); jack_elias@brown.edu (J.A.E.)

Published 11 June 2014, *Sci. Transl. Med.* **6**, 240ra76 (2014)
DOI: 10.1126/scitranslmed.3007096

The PDF file includes:

macrophages, and CD206^{lo} macrophages obtained from bleomycin-exposed mouse lungs.
Table S1. Characteristics of subjects for CHI3L1 analysis.
Table S2. Characteristics of subjects for CD206 analysis.
Table S3. Characteristics of progressive and stable IPF subjects for CD206 analysis.

Supplemental Figure S1.

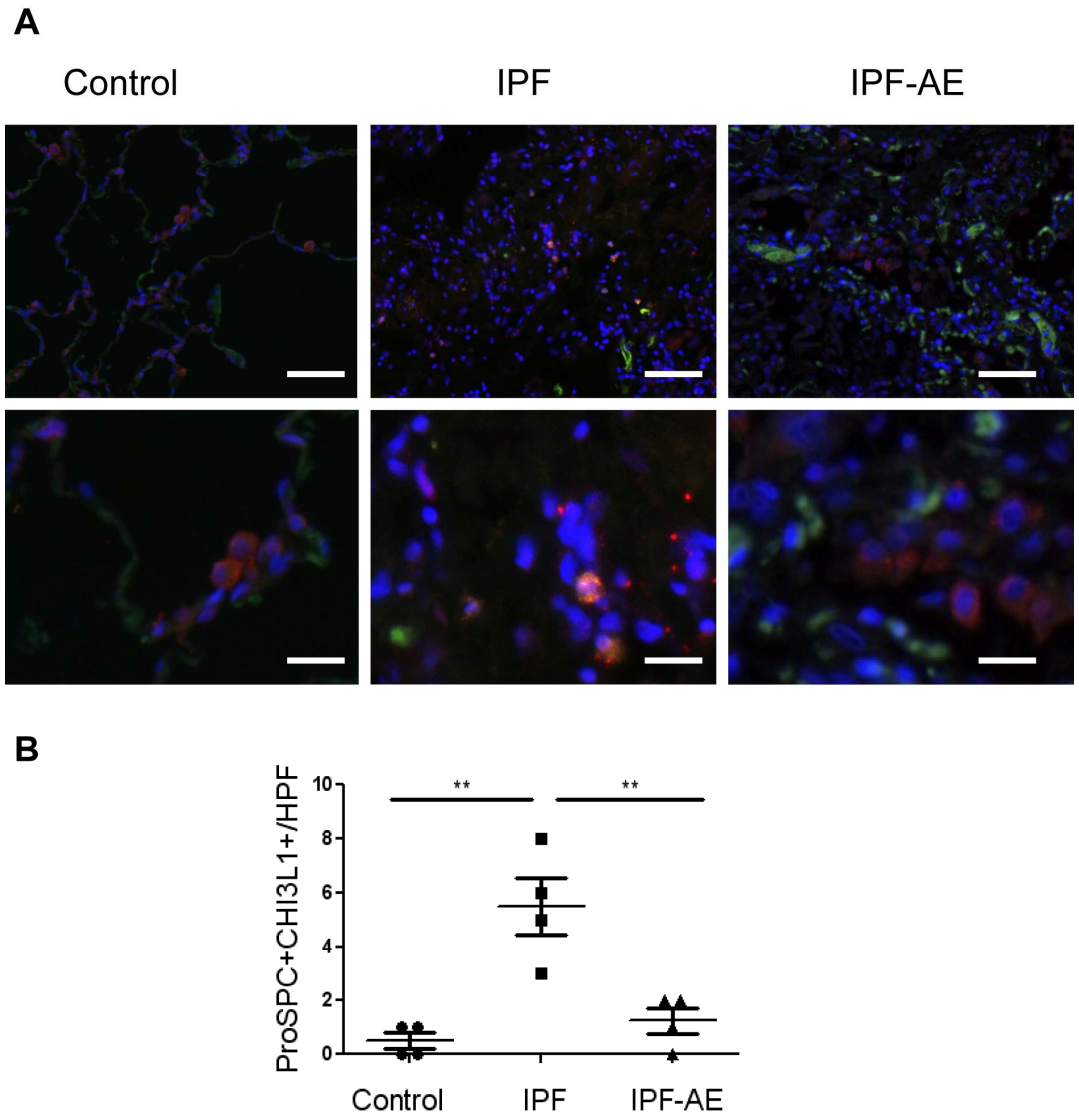

Supplemental Figure S1. Colocalization of CHI3L1 and pro-SPC in the human lung. A. Sections obtained from contol and IPF lung biopsies, and autopsy specimens from IPF-AE, underwent immunofluorescence colocalization of pro-SPC (red cytoplasmic signal), CHI3L1 (green), and were counterstained with DAPI (blue). Compared to control (leftmost panel) in which there was only scant colocalization of these markers, IPF lung biopsies demonstrate many cells exhibiting both pro-SPC and CHI3L1 (middle panel) that are absent in the setting of IPF-AE (rightmost panel). Scale bar is 100 microns in the top images and 50 microns in the bottom images. B)Quantitative comparison of cells expressing both pro-SPC and CHI3L1 reveals significant increases in IPF lung biopsies (n = 4) compared to normal (n = 4) and IPF-AE (n=4) ($p<0.01$ for both comparisons using one way ANOVA with Bonferroni post test) .

Supplemental Figure S2.

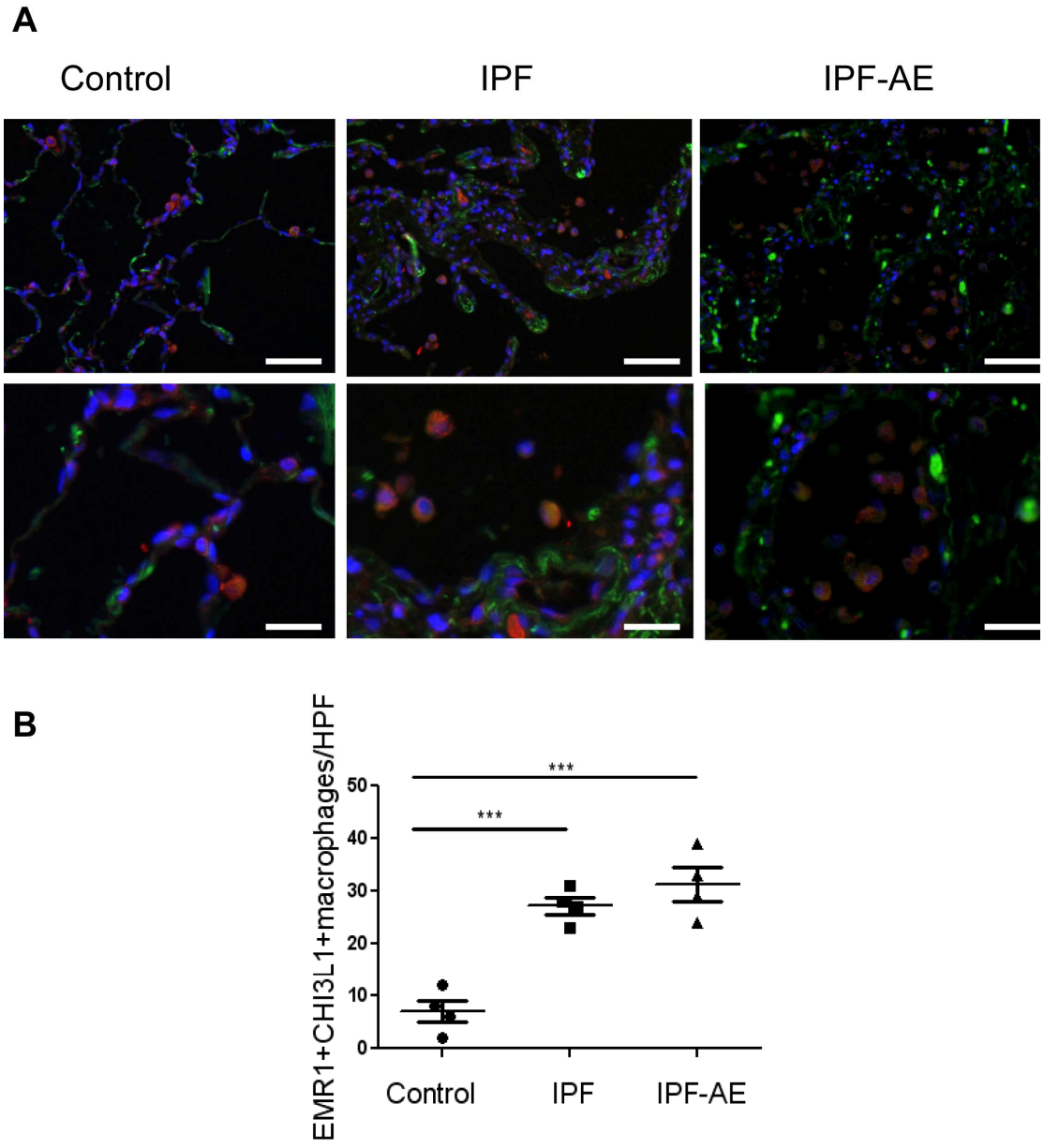

Supplemental Figure S2. Colocalization of CHI3L1 and EMR-1 in the human lung. A. Sections obtained from contol and IPF lung biopsies, and autopsy specimens from IPF-AE, underwent immunofluorescence colocalization of EMR-1 (red cytoplasmic signal), CHI3L1 (green), and were counterstained with DAPI (blue). Compared to control (leftmost panel) in which there was only scant colocalization of these markers, both IPF lung biopsies and autopsy specimens from IPF-AE demonstrate many cells with the morphology of alveolar macrophages exhibiting both EMR-1 and CHI3L1 (middle panel and rightmost panels respectively). Scale bar is 100 microns in the top images and 50 microns in the bottom images. B)Quantitative comparison of cells expressing both EMR-1 and CHI3L1 reveals significant increases in both IPF lung biopsies (n = 4) and IPF-AE (n=4) when compared to control (both comparisons $p<0.001$ using one way ANOVA with Bonferroni post –test).

Supplemental Figure S3.

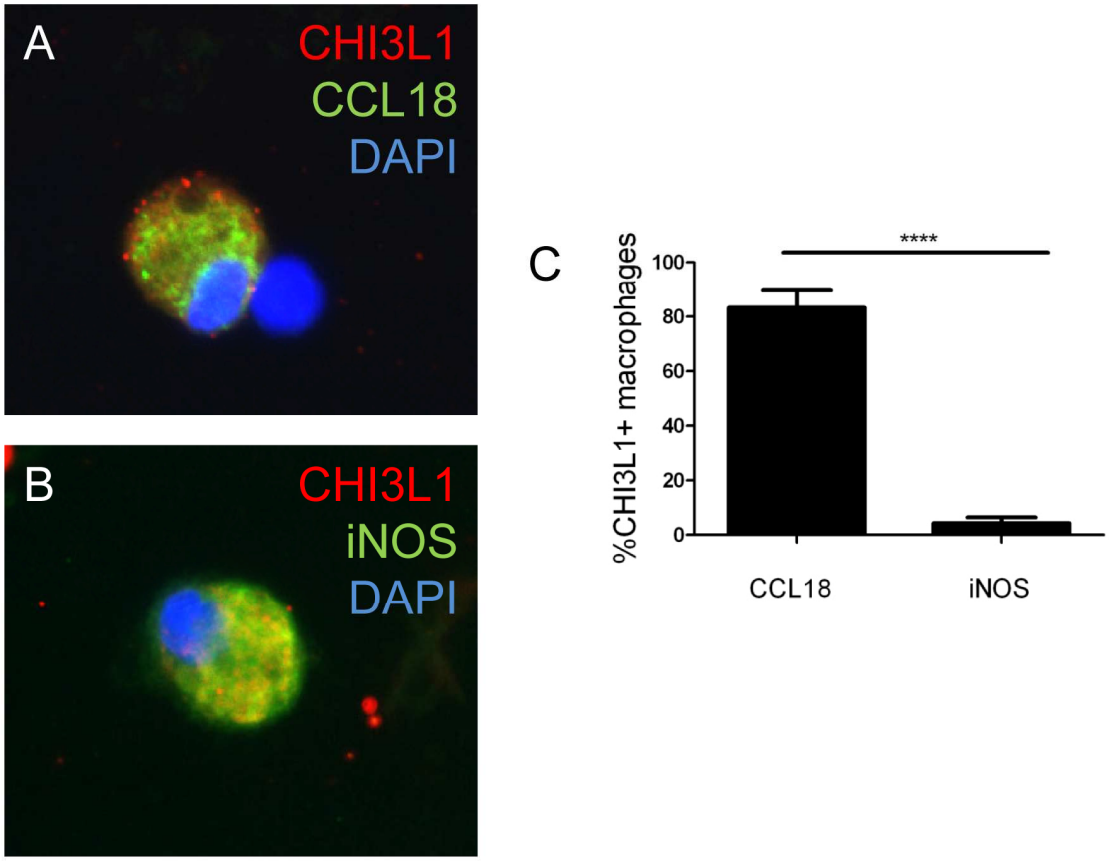

Supplemental Figure S3. Immunoflourescence analysis of IPF lung cytospins demonstrates that Texas red–labeled CHI3L1 (red) colocalizes with (A) CCL18 (green) and (B) iNOS (green). Cells are counterstained with DAPI (blue) in both images. C) Semiquantitative comparison of costaining reveals a more than ten-fold increase in CCL18 expression by CHI3L1+ macrophages compared to iNOS ($p<0.0001$, Student's unpaired t-test, n=3 per group).

Supplemental Figure S4.

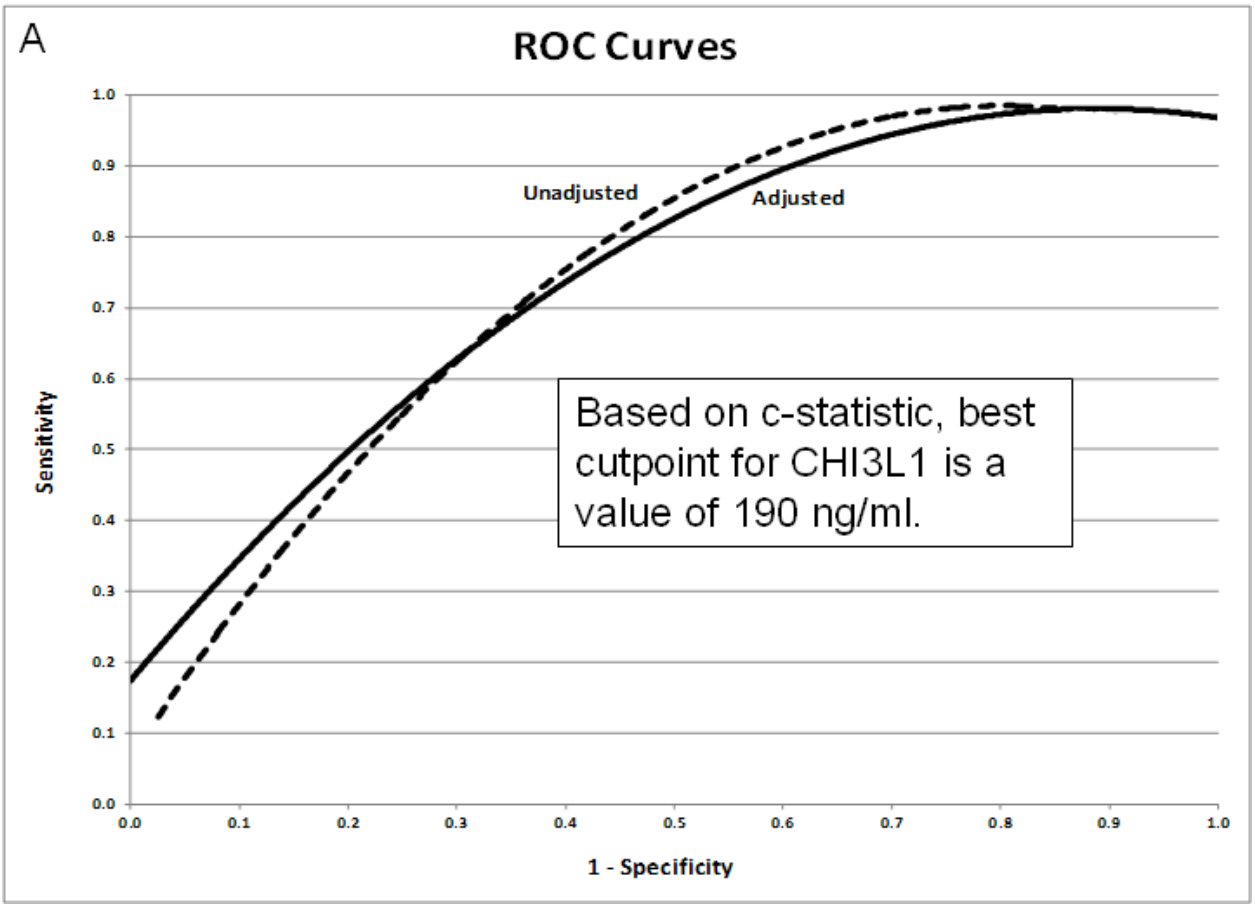

Supplemental Figure S4. Logistic regression modeling was used to calculate an unadjusted ROC curve as well as an ROC curve adjusted for age, gender, %FVC predicted at baseline, and corrected DLCO. The C-statistic was calculated for various split points in the continuous variable YKL40 to determine the optimal split point. Values range from 0.5 (indicating the model is no better than chance for, in our case, detecting event free survival at 504 days) to 1.0 (indicating the model perfectly identifies those subjects which will be event free at 504 days). Results from this analysis indicate that a plasma concentration of 190 ng/ml most robustly differentiates stable from progressive subjects.

Supplemental Figure S5.

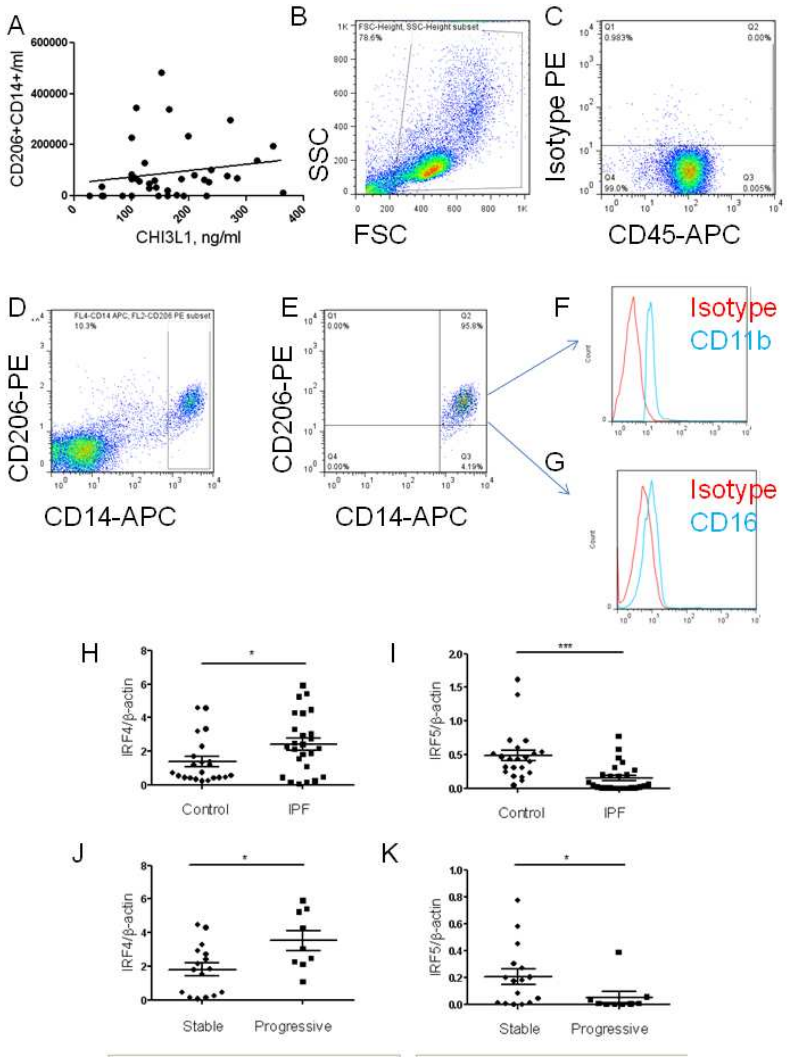

Supplemental Figure S5. Relationship of CD206 monocytes and CHI3L1 in the IPF circulation. A) Circulating CD206 concentrations (*y* axis) with plasma CHI3L1 concentrations (*x* axis) show a weak positive correlation (Spearman $r = 0.39$, $P = 0.013$). B-G. FACS gating on CD14+CD206+ cells. B)Live cells are selected based on forward (FSC) vs. side scatter (SSC). C. The negative gate for PE on APC+ cells is set based on appropriate positive and isotype controls. D. CD14+ cells are gated upon and (E) percentages of CD206+ cells are obtained by setting the gate established in C. Further analysis of this population in a small group of IPF subjects finds the CD14+CD206+ cells are shifted to the right in the CD11b channel but not the CD16 channel. H-K. q-RTPCR based assessed of macrophage-associated transcription factors reveals that compared to control subjects (n=21), PBMCs obtained from IPF subjects (n=25) display (H) increased relative expression of the M2-associated transcription factor IRF-4 ($p = 0.0392$, Mann-Whitney comparison) and (I) reduced expression of the M1-associated transcription factor IRF-5 ($p<0.0001$, Mann-Whitney comparison). Further analysis of the IPF subjects reveals that relative to those with stable disease (n = 16) in progressive subjects (n=9) IRF-4 expression is increased ($p=0.0151$, Student's unpaired t-test) (J) and IRF-5 expression is decreased ($p=0.0292$, Mann-Whitney comparison) (K).

Supplemental Figure S6.

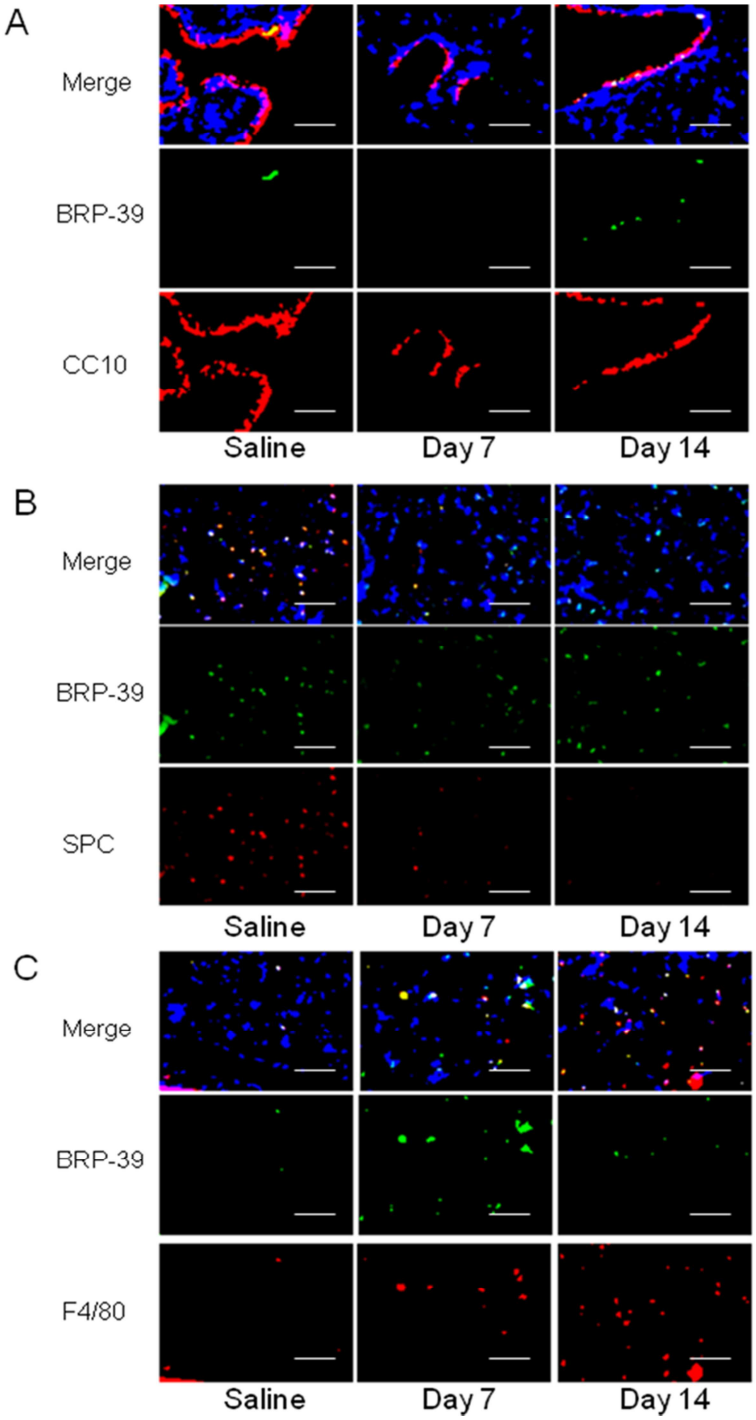

Supplemental Figure S6. Localization of CHI3L1 expression. WT mice were subjected to intratracheal bleomycin administration and lung sections were stained for CHI3L1(BRP-39) (green). Sections were co-stained for CC10 (A), SPC (B), or F4/80 (C). Images are representative of 3 mice. Scale bar is 200 microns.

Supplemental Figure S7.

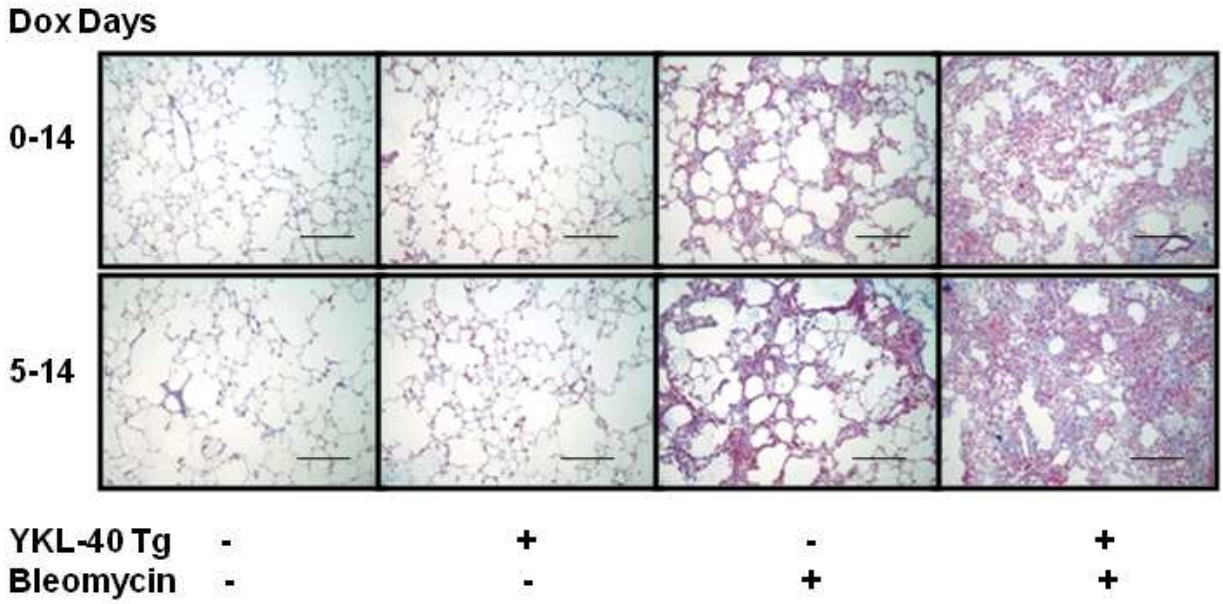

Supplemental Figure S7. CHI3L1 regulates collagen deposition in a temporally specific manner. WT and YKL-40 Tg mice were subjected to intratracheal bleomycin administration and YKL-40 Tg was turned on from days 0-14 (top) or days 5-14 (bottom). Trichrome staining was performed to examine collagen deposition. Images are representative of a minimum of 4 mice in each group. Scale bar is 200 microns.

Supplemental Figure S8.

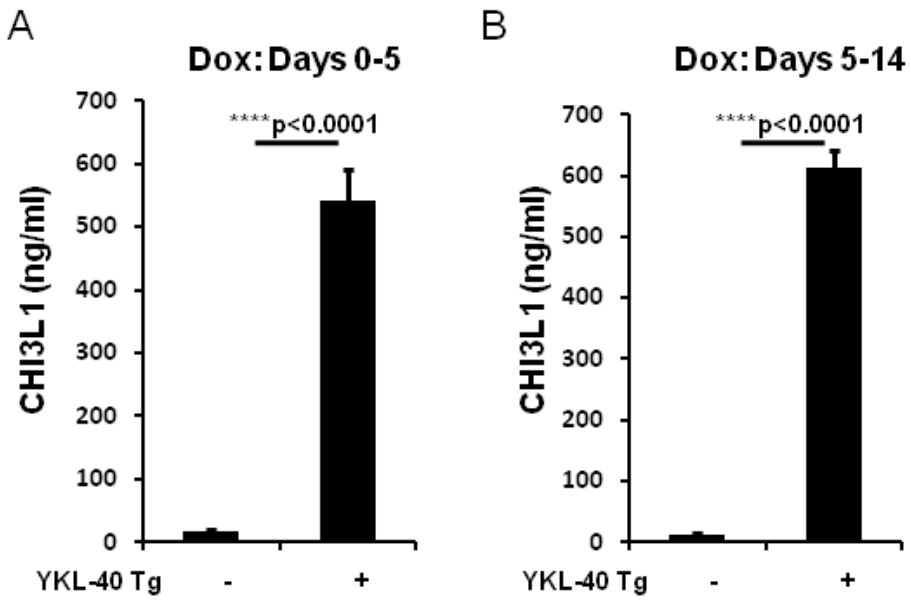

Supplemental Figure S8. CHI3L1 transgene is induced with doxycycline. (A) Bleomycin was administered two days after the induction of YKL-40 Tg expression. YKL-40 Tg production in BAL fluid was quantified using ELISA on Day 7. Compared to identically treated controls (n=4), YKL-40 levels are increased in bleomycin treated YKL-40 Tg mice (n=4). P=0.00004, unpaired Student's t-test. (B) YKL-40 Tg expression was induced from Day 5 to Day 14 following intratracheal bleomycin. YKL-40 Tg production in BAL fluid was quantified using ELISA on Day 14. Compared to controls (n=4), YKL-40 levels are increased in YKL-40 Tg mice (n=4). P=0.00002, unpaired Student's t-test.

Supplemental Figure S9.

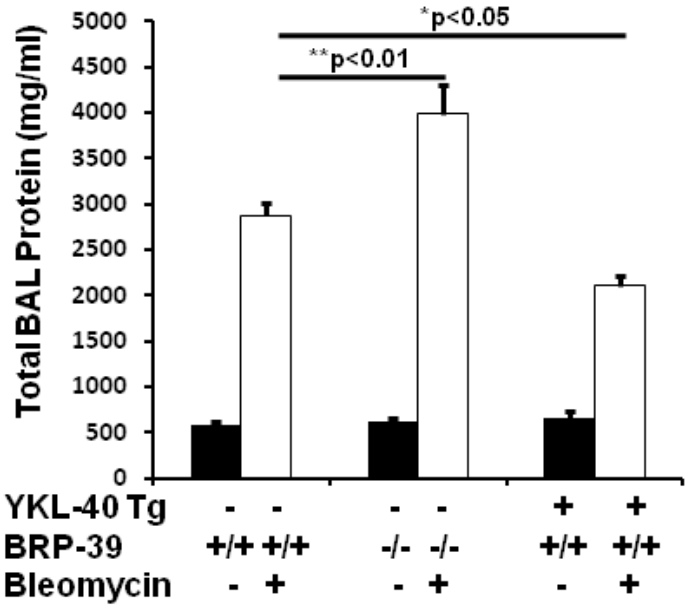

Supplemental Figure S9. Alveolar injury is increased in BRP-39$^{-/-}$ mice and is decreased in YKL-40 Tg mice. Bleomycin was administered two days after the induction of YKL-40 Tg expression. BAL fluid was collected and total protein concentration was quantified using Bradford assay on Day 7. Compared to controls (n=4), BAL protein levels are increased in BRP-39$^{-/-}$ mice (n=4). P=0.004, unpaired Student's t-test. BAL protein levels are decreased in YKL-40 Tg mice (n=4). P=0.03, unpaired Student's t-test.

Supplemental Figure S10.

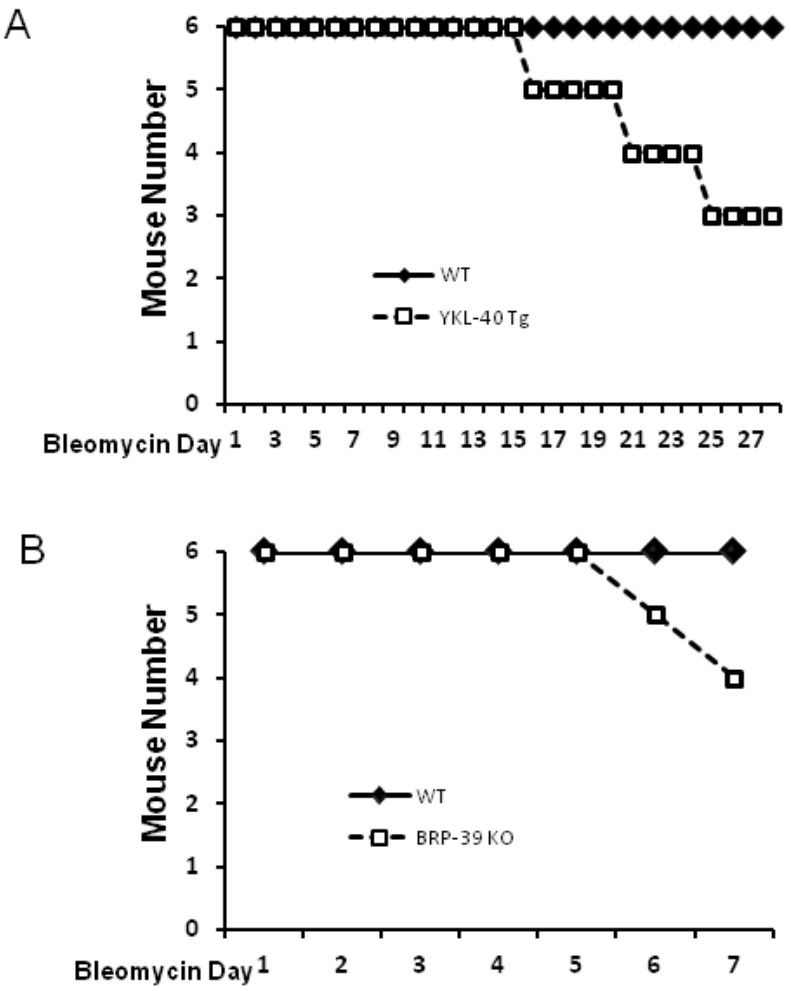

Supplemental Figure S10. Mortality data. (A) WT and YKL-40 Tg mice were treated with bleomycin. YKL-40 Tg expression was induced from Day 5 to the end of the experiment and mortality was assessed during the fibroproliferative repair phase. (B) WT and BRP-39$^{-/-}$ mice were treated with Bleomycin and mortality was assessed in the injury phase. N=6 in each group.

Supplemental Figure S11.

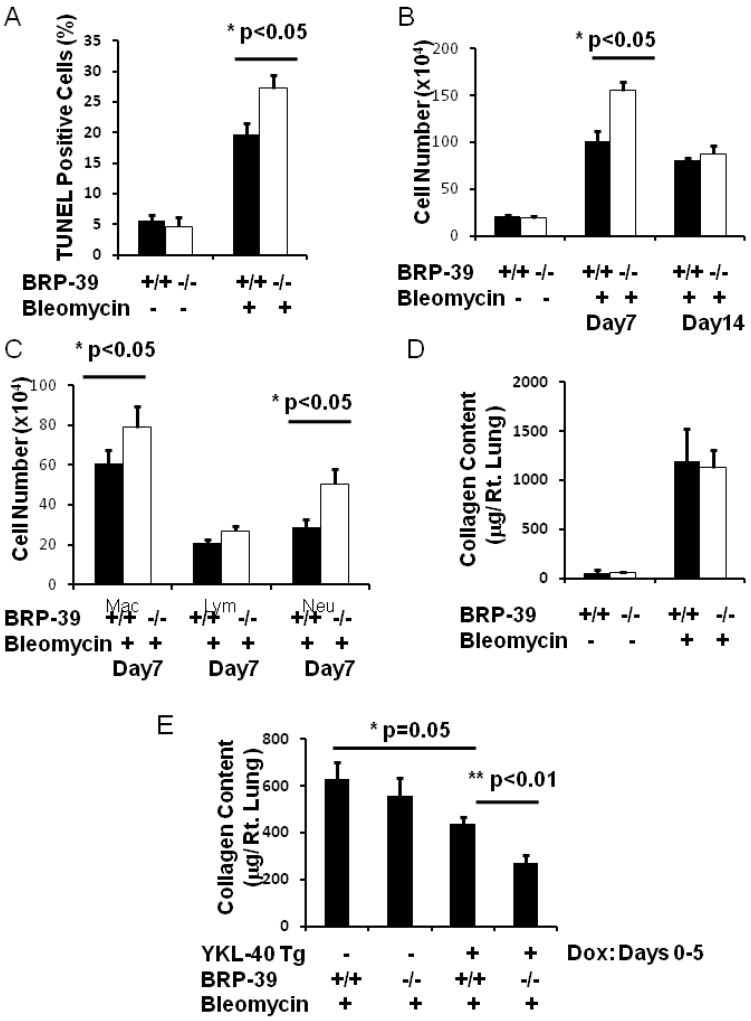

Supplemental Figure S11. Wild-type and BRP-39 mutant mice were subjected to intratracheal bleomycin administration. (A) TUNEL positive cells were counted on Day 7. Compared to controls (n=4), TUNEL positive cells are increased in BRP-39$^{-/-}$ mice (n=4). P=0.019, unpaired Student's t-test. (B) BAL inflammation was determined on Day 7 and Day 14. Compared to controls (n=4), total BAL cells are increased in BRP-39$^{-/-}$ mice (n=4) on Day 7. P=0.03, unpaired Student's t-test. (C) Cytospins of lung BAL revealed that compared to controls (n=4), macrophages are increased in BRP-39$^{-/-}$ mice (n=4) on Day 7. P=0.045, unpaired Student's t-test. Neutrophils are also increased in BRP-39$^{-/-}$ mice on Day 7. P=0.02, unpaired Student's t-test. (D) Total lung collagen was quantified using Sircol assay on Day 14. No statistical significance was found. (E) BRP-39 null mice were bred to YKL-40 Tg background, and YKL-40 Tg were activated only during tissue injury phase (Days 0-5). Total lung collagen was quantified using Sircol assay on Day 14. Compared to WT mice (n=4), total lung collagen is decreased in YKL-40 Tg mice (n=4). P=0.05, unpaired Student's t-test. Compared to YKL-40 Tg mice (n=4), total lung collagen is decreased in YKL-40 Tg/BRP-39$^{-/-}$ mice (n=4). P=0.003, unpaired Student's t-test.

Supplemental Figure S12.

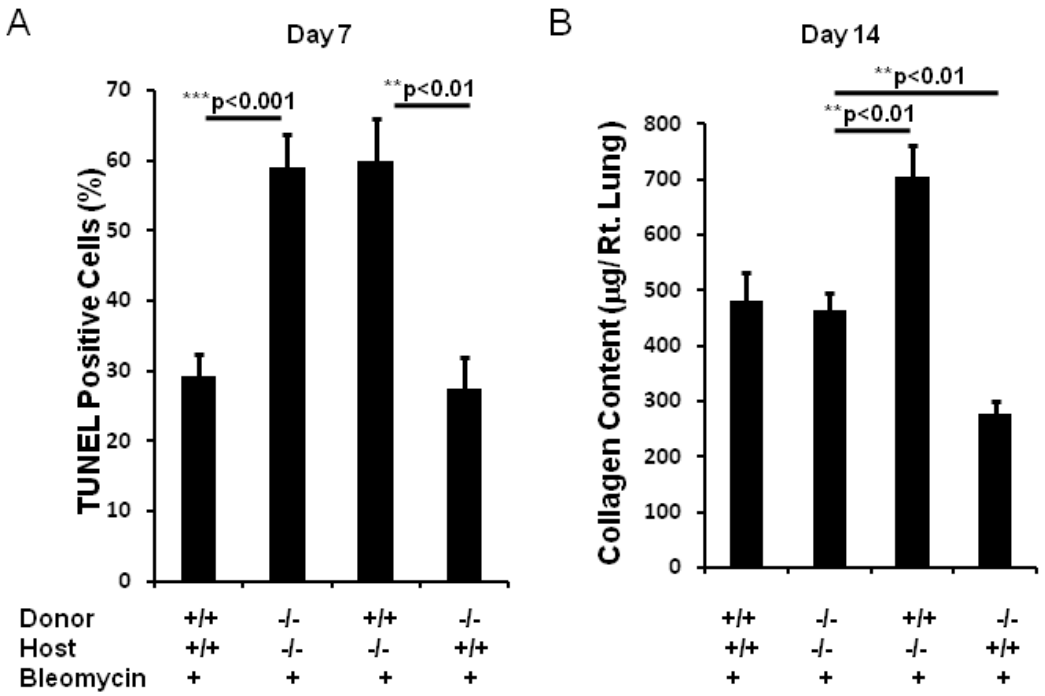

Supplemental Figure S12. Structural cell–derived CHI3L1 is required to prevent cell death, and bone marrow–derived CHI3L1 amplifies lung fibrosis. Bone marrow chimeras were generated between WT and BRP-39$^{-/-}$ (KO) mice, mice were subjected to intratracheal bleomycin administration. (A) TUNEL positive cells were counted on Day 7. Compared to WT-WT mice (n=4), TUNEL positive cells are increased in KO-KO mice (n=4). P=0.0009, unpaired Student's t-test. Compared to WT-KO mice (n=4), TUNEL positive cells are decreased in KO-WT mice (n=4). P=0.004, unpaired Student's t-test. (B) Total lung collagen was quantified using Sircol assay on Day 14. Compared to KO-KO mice (n=4), total lung collagen is increased in WT-KO mice (n=4). P=0.002, unpaired Student's t-test. Compared to KO-KO mice (n=4), total lung collagen is decreased in KO-WT mice (n=4). P=0.009, unpaired Student's t-test.

Supplemental Figure S13.

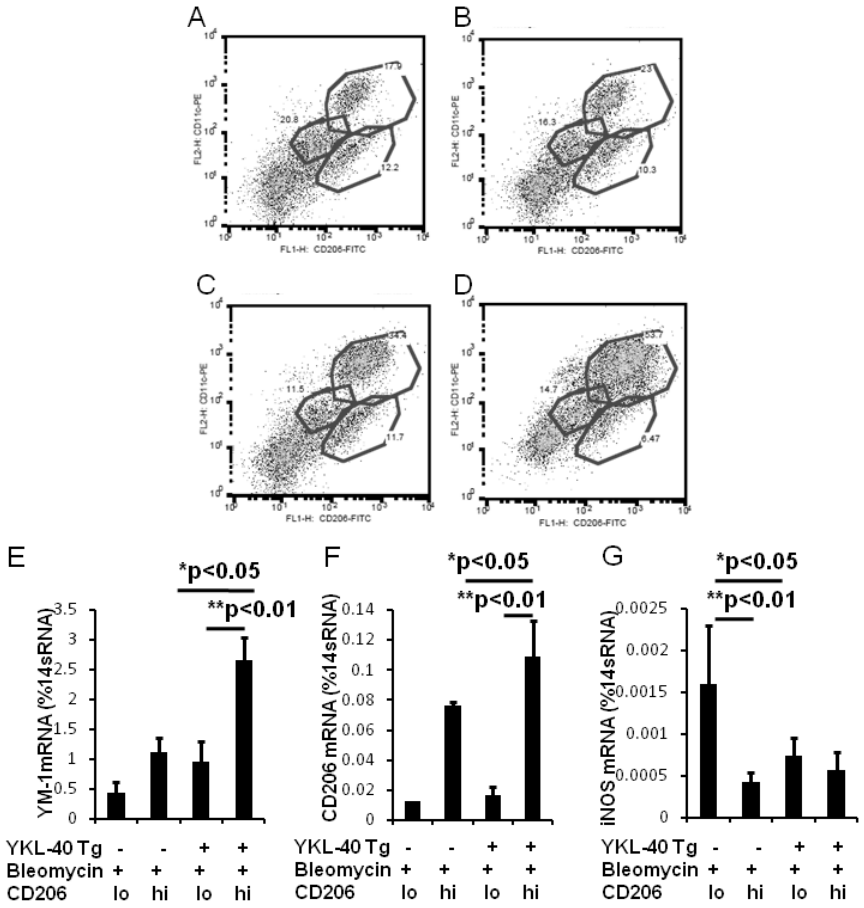

Supplemental Figure S13. Wild-type and YKL-40 Tg mice underwent intratracheal bleomycin administration, and YKL-40 Tg activated from days 5 to 14. FACS was used to analyze CD11c and CD206 expression on a CD45+F4/80+ gated population from lungs of (A) saline-treated WT mouse, (B) saline-treated YKL-40 Tg mouse., (C) bleomycin-treated WT, (D) bleomycin-tretaed YKL-40 Tg. X-axis: CD206; Y-axis: CD11c. CD45+F4/80+CD11C+CD206+($CD206^{hi}$) cells were sorted from CD45+F4/80+CD11C-CD206-($CD206^{lo}$) cells. mRNA levels of (E) YM-1, (F) CD206, and (G) iNOS were evaluated by qRT-PCR on RNA extracted from these cells. Compared to $CD206^{lo}$ cells (n=4), YM-1 is increased in $CD206^{hi}$ cells (n=4). P=0.006, unpaired Student's t-test. Compared to $CD206^{hi}$ cells from WT mice (n=4), YM-1 is increased in $CD206^{hi}$ cells from YKL-40 Tg mice (n=4). P=0.012, unpaired Student's t-test. Compared to $CD206^{lo}$ cells (n=4), CD206 is increased in $CD206^{hi}$ cells (n=4). P=0.002, unpaired Student's t-test. Compared to $CD206^{hi}$ cells from WT mice (n=4), CD206 is increased in $CD206^{hi}$ cells from YKL-40 Tg mice (n=4). P=0.04, unpaired Student's t-test. Compared to $CD206^{lo}$ cells (n=4), iNOS is decreased in $CD206^{hi}$ cells (n=4). P=0.009, unpaired Student's t-test. Compared to $CD206^{lo}$ cells from WT mice (n=4), iNOS is decreased in $CD206^{lo}$ cells from YKL-40 Tg mice (n=4). P=0.02, unpaired Student's t-test.

Supplemental Figure S14.

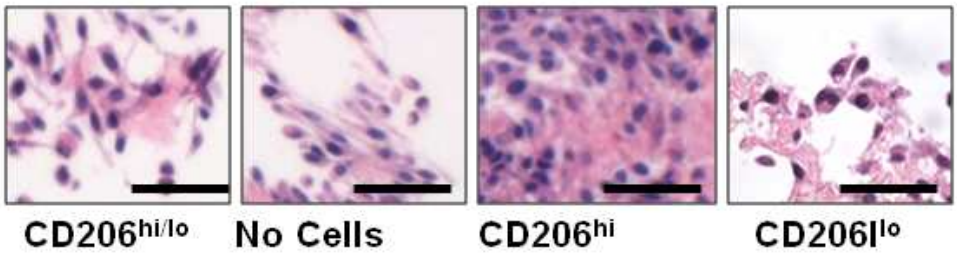

Supplemental Figure S14. H&E images of fibroblast-seeded mouse lung scaffolds grown in the presence of (left to right) $CD206^{hi/lo}$ macrophages, no macrophages, $CD206^{hi}$ macrophages, and $CD206^{lo}$ macrophages obtained from bleomycin-exposed mouse lungs. Scale bar is 50 microns.

Table S1. Characteristics of subjects for CHI3L1 analysis.

	IPF N=64	Control N=42	P value
Age, years	70.75 (63.69-76.36)	69.00 (65.00- 76.00)	0.8946
Sex Female Male	9(14.06%) 55 (85.94%)	22 (52.38%) 20 (47.62%)	0.0004
Race Caucasian Not Caucasian	55(85.94%) 9(14.06%)	38 (90.5%) 4 (9.5%)	0.76
FVC, Percent Predicted	63.70 (59.82 – 67.58)	NA	NA
DLCO, Percent Predicted	43.32 (39.68 – 46.98)	NA	NA

Data are expressed as mean with 95% confidence intervals.
FVC = forced vital capacity. DLCO = diffusion capacity for carbon monoxide.

Table S2. Characteristics of subjects for CD206 analysis.

	IPF N=38	Control N=42	P value
Age, years	69.76 (59.97– 71.30)	65.60 (59.9 - 71.3)	0.2088
Sex Female Male	 8 (21.05%) 30(78.95%)	 22 (52.4%) 20 (47.6%)	 0.0038
Race Caucasian Not Caucasian	 34 (89.47%) 4 (10.53%)	 38 (90.5%) 4 (9.5%)	 0.2850
FVC, Percent Predicted	67.05 (62.47– 71.63)	NA	NA
DLCO, Percent Predicted	44.00 (39.13- 48.86)	NA	NA

Data are expressed as mean with 95% confidence intervals.
FVC = forced vital capacity. DLCO = diffusion capacity for carbon monoxide.

Table S3.Characteristics of progressive and stable IPF subjects for CD206 analysis.

	Progressive N=11	Stable N=27	P value
Age, years	72.71 (69.6813 – 75.7411)	68.22 (64.0894 - 72.3618)	0.1394
Sex Female Male	 2 (15.38%) 11 (84.62%)	 6 (24.00%) 19 (76.00%)	0.5366
Race Caucasian Not Caucasian	 12 (92.31%) 1 (7.69%)	 22 (88.00%) 3 (12.00%)	0.6814
FVC, Percent Predicted	65.38 (57.89 – 72.86)	67.92 (61.79 - 74.04)	0.5808
DLCO, Percent Predicted	42.38 (30.80 - 53.96)	44.8400 (39.74- 49.93)	0.6804
Outcome Transplant Death	 5 6		

Data are expressed as mean with 95% confidence intervals.
FVC = forced vital capacity. DLCO = diffusion capacity for carbon monoxide.